Measurements of the ^{210g}Bi to ^{210m}Bi activation ratio for the ^{209}Bi(n,γ) reaction with thermal and epithermal neutrons at the Soreq IRR1 reactor

A. Shor,[1] L. Weissman,[1] M. Tessler,[1] O. Aviv,[1] Y. Eisen,[1] G. Feinberg,[1] Y. Mishnayot,[1,2] A. Plompen,[3] and S. Vaintraub[1]

[1]*Soreq Nuclear Research Center, Yavne 81800, Israel*

[2]*Racah Institute of Physics, Hebrew University, Jerusalem 91904, Israel*

[3]*European Commission, Joint Research Centre, 2440 Geel, Belgium*

(Received 3 October 2021; accepted 7 January 2022; published 7 February 2022; corrected 15 February 2022)

Irradiations of bismuth samples with thermal and epithermal neutrons have been performed for a comparison of activation to the ^{210g}Bi ground state and to the ^{210m}Bi metastable state. The bismuth irradiations were conducted at the Soreq IRR1 research reactor at a near-core location with integrated neutron flux of approximately 2×10^{18}neutrons/cm^2 and a gold cadmium ratio of 3.1. Two nearly identical bismuth samples were irradiated, one without and one with a cadmium shield, to enable a comparison between thermal and epithermal neutron capture cross sections. Subsequent gamma spectrometry indicates nearly equal levels of activation to the ground and to the metastable states of ^{210}Bi, both with thermal and epithermal neutrons. Absolute thermal cross sections and resonant integrals were deduced by including previously reported bismuth activation measurements performed conjointly with gold foil activation for normalization. A comparison of the present results with existing data is presented. It is argued that the bismuth resonances lie in the neutron energy range relevant for stellar temperatures, and therefore the neutron capture cross section ratio (σ_g/σ_m) measured for the epithermal neutrons is relevant also for stellar ^{210}Bi production. This is of importance since bismuth lies at the end of the chain for the *s-process* reaction for nucleosynthesis in stars. Precise knowledge of bismuth activation to the ^{210m}Bi metastable state is also vital for the planning of GEN-IV reactors given the 3-million-yr half-life of ^{210m}Bi.

DOI: 10.1103/PhysRevC.105.025802

I. INTRODUCTION

Neutron activation studies of bismuth have been employed at both accelerator and reactor facilities for measurements of astrophysical processes and for planning of Gen-IV reactors and safety systems. Reactor measurements of neutron activation of bismuth have been performed with cold and thermal [1], intermediate energy and fast neutrons [2]. Accelerator measurements with neutrons produced by pulsed electron [3] or by pulsed proton [4] beams have enabled accurate time-of-flight (TOF) measurements and neutron activation studies in the resonance region and beyond. Accelerator studies have employed the $p + \mathrm{Li}$ reaction near threshold to produce neutrons with quasi-Maxwellian distribution at $kT \approx 30$ keV [5] and thereby enable activation studies of bismuth with astrophysical relevant neutron distribution [6–8]. There is a need for improving the accuracy and consistency between these measurements, especially regarding comparisons between activation to the ^{210g}Bi ground state and the ^{210m}Bi metastable state [9].

Neutron capture on ^{209}Bi ($I^\pi = 9/2^-$) is followed by the emission of characteristic prompt gammas that allow determining the yields of ^{210g}Bi and ^{210m}Bi, separately. The ground state ^{210g}Bi ($I^\pi = 1^-$) decays to ^{210}Po with a half-life of 5.012 days, and the ^{210}Po subsequently α decays to ^{206}Pb with a 138-day half-life. A small fraction [branching ratio of $1.15(9) \times 10^{-5}$] of the ^{210}Po decays to the ^{206*}Pb excited state, with the subsequent emission of a γ ray with energy of 803 keV. The second possibility is creation of a long-lived isomer ^{210m}Bi ($I^\pi = 9^-$), a metastable state at excitation energy of 271 keV, that α decays to ^{206*}Tl with a 3-million-yr half-life. The ^{206*}Tl de-excites to the ground state by emitting several gammas, primarily at 265.6 and 304.6 keV. Figure 1 shows the scheme for neutron capture on bismuth with the possible decay schemes [10,11].

The importance of neutron activation of bismuth for astrophysical processes relies on bismuth being the last nuclide along the *s-process* reaction path for nucleosynthesis of the heavy elements in stellar environments [5]. Neutron capture on bismuth and beyond populates α-unstable isotopes contributing to the recycling of lighter nuclides involved in the *s* process. Measurements of neutron capture on bismuth in the astrophysical neutron energy range involving TOF techniques, along with measurement of the prompt gammas, provide a lower limit of the total neutron capture cross section on bismuth. Activation of bismuth with a quasi-Maxwellian neutron spectrum and subsequent off-line measurement of the 803-keV gamma line leading to ^{206}Pb, provide absolute measurements, but only for activation to the ^{210}Bi ground state. Direct measurements of activation to the ^{210}Bi metastable state are also required. Despite the large gamma fluxes in stellar environment and the small energy gap between the ^{210g}Bi and ^{210m}Bi states, the difference in spin parity precludes a high transition rate between these two states, even in a gamma-rich

 ©2022 American Physical Society

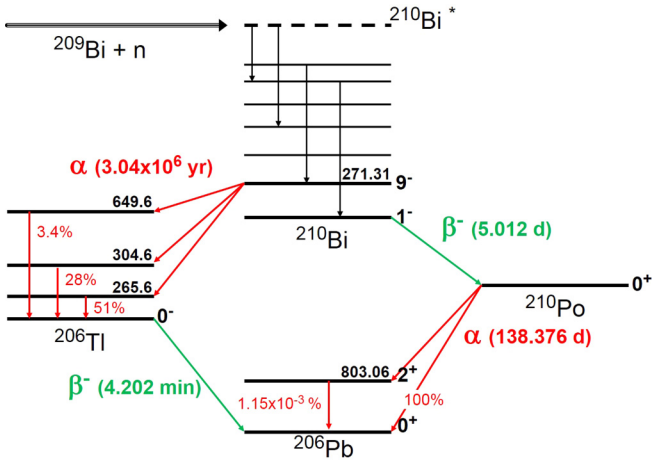

FIG. 1. Decay scheme following neutron capture on ^{209}Bi. Energy level data from [10,11].

stellar thermal environment. More precise measurements of neutron capture on bismuth are therefore needed for a more complete picture of the abundances near the end of the *s* process, especially for the ratio of activation to the ground state and the metastable states of ^{210}Bi. Knowledge of *s*-process abundances is also crucial for assessing radiogenic contributions due to Th/U decay and its use as cosmochronometers [12].

Several designs for GenIV reactors involve eutectic Pb-Bi mixtures as reactor coolants [13] or as high power targets for intense proton/deuteron beams for accelerator driven systems (ADSs) [14]. The Pb-Bi mixture has the advantageous properties of low melting and high boiling point temperatures, in addition to chemical inertness, and low neutron absorption but large scattering cross sections. It is therefore a very appropriate material for use as reactor coolants or for spallation targets for accelerator driven systems. However, neutron capture on bismuth makes the eutectic mixtures radiotoxic due to the ^{210}Po decay product and long-lived radiotoxicity due to the ^{210m}Bi isomer created. More precise data on neutron bismuth activation, especially leading to the long-lived isomer, is therefore critical for safe and reliable reactor design.

A bismuth activation measurement with quasi-Maxwellian neutrons has been previously reported by this group, with emphasis on the Maxwellian averaged cross section (MACS) for activation to the ^{210g}Bi ground state [8]. This group has also recently reported on an accurate measurement of the small decay branching ratio to the 803-keV gamma following the decay of ^{210g}Bi [15], which is also very important for the determination of the MACS. However, the measurement of activation to the bismuth-210 metastable state ^{210m}Bi has been extremely difficult due to the long half-life of the isomer. A careful measurement of activation to the metastable state is therefore warranted.

Recently, Al-Khasawneh *et al.* [2] have reported on a new determination of the ^{209}Bi$(n,\gamma)^{210}$Bi cross section for thermal neutrons and for the Maxwellian averaged cross section (MACS) at 30 keV. Comparing two irradiated samples, one with and one without a cadmium shield, they measured the thermal capture cross section, as well as the resonant integral. In their paper, Al-Khasawneh *et al.* emphasize that despite the numerous bismuth activation measurements already reported, there is a need for more accurate data.

In this paper we report on activation studies of bismuth samples with thermal and epithermal neutrons and a comparison of activation to the ^{210g}Bi ground state versus activation to the ^{210m}Bi metastable state. The bismuth irradiations were carried out at the Soreq IRR1 research reactor at a near-core location with gold cadmium ratio of 3.1, with two nearly identical bismuth samples, one with and one without a cadmium shield to enable a comparison between thermal and epithermal neutron activation. Absolute thermal capture cross sections and resonant integrals, for activation to both ^{210g}Bi and ^{210m}Bi, were obtained by referring to previously reported activation measurements performed concurrently with a gold foil for normalization, as reported by this group [15]. The results are compared to existing measurements reported in the literature. It is argued that the epithermal activation of bismuth lies in the neutron energy range relevant to astrophysical processes, and therefore the ratio $(\sigma_g/\sigma_m)_{\rm epi}$ obtained for activation to the ground state versus activation to the metastable state measured with the epithermal neutrons, is also indicative of the ratio for the astrophysical Maxwellian averaged cross section (MACS) reactions.

For the purpose of this work, the thermal neutrons are defined as those with energy below the cadmium energy cutoff of 0.5 eV, and epithermal neutrons are those with energy above the cadmium energy cutoff. This usage of the thermal and epithermal terminology for comparison of irradiation of cadmium unshielded and shielded samples has been used by many authors in various contexts. A sample of papers that define thermal and epithermal neutron energy regions as those without and with a cadmium shield is included in Refs. [2,15–17]. As will be demonstrated later, the so called epithermal neutrons relevant for this work cover the range 0.5 eV–2 MeV.

II. IRRADIATION

The bismuth irradiations took place at the Soreq IRR1 research reactor [18]. The irradiations were performed using hyperpure bismuth discs of 99.9999% purity [19]. Two bismuth discs were simultaneously irradiated near the IRR1 reactor core at a location with approximate thermal neutron flux of 2.5×10^{13} neutrons/cm^2/s. Each bismuth disc was 8 mm in diameter and 1 mm thick, and weighed 0.484(4) g. Each was placed in a separate quartz flask, where one of the flasks was covered with a 0.5-mm-thick cadmium foil. The flasks were placed end to end lengthwise in a known location near the core at a known flux and gold cadmium ratio of 3.1. The irradiations took place during April of 2015, and were divided into three separate irradiations, where the total irradiation time was about 20 h. The details of the three irradiations are listed in Table I. The quantity $t_{\rm cool}$ represents cooling time, the number of days from the end of the third irradiation, and the beginning of the gamma spectroscopy measurement of the sample. The quantity $t_{\rm irr}$ is the length of the irradiation, and Δt is the time between the end of each irradiation and the beginning of $t_{\rm cool}$ ($\Delta t = 0$ for the third irradiation). For

TABLE I. Bismuth samples irradiation cycle.

Irradiation	t_{irr} = length of irradiation (days)	Δt = time to beginning of t_{cool} (days)
1	0.304	8.96
2	0.300	1.99
3	0.275	0.0

each of the irradiations the reactor was operated at the same power level (uncertainty of ±7.5%) so that the amount of irradiation is proportional to t_{irr}. At the end of the irradiations, the samples were removed, and gold foils with and without cadmium shield were placed at the same irradiation location and the known gold cadmium ratio of 3.1 was confirmed. Table I summarizes the irradiations.

III. MEASUREMENT OF GAMMA ACTIVITY

Several measurements of the gamma activity were performed for each irradiated bismuth sample. Activity of the 803-keV line provided information on the activation to the ^{210g}Bi ground state, and activity of the 265.6- and 304.6-keV lines provided the activation to the ^{210m}Bi metastable state. After the irradiations and one month of cooling, the irradiated bismuth disks were encapsulated in specially made holders designed for precise and reproducible placement to accommodate the horizontal cryostat configuration of the High Purity Germanium (HPGe) detector [20]. The activation measurements were performed with the bismuth samples placed in contact with the HPGe detector window for the duration of the activation measurement. The measurements presented in this analysis were performed approximately 2.23 yr after the irradiation, where the 803-keV line was still prominent, and where short-lived activation of impurities in the bismuth samples had sufficient time to decay to avoid contamination in the region of the metastable lines. Measurements of gamma activity were performed separately for samples without and with a cadmium shield, using the same HPGe detector and holder configuration. Additional shorter measurements were performed both following the irradiation and 3–4 yr after the irradiation to demonstrate the consistency of the data. These shorter measurements did not improve accuracy significantly, which were mostly dominated by systematic uncertainties, but did allow us to ascertain that the data consistency remained intact. Table II describes the main measurements, where t_{cool} is the time from the end of the last irradiation to the beginning of the gamma activation measurement, and t_{meas} is the length of time for the activation measurement. The measurement time for the sample with Cd shield was slightly longer to approximately compensate for the later measurement. Figure 2 shows the overall gamma spectrum acquired for the main measurements for the irradiated bismuth samples with and without the cadmium shields.

TABLE II. Bismuth samples measuring time.

	t_{cool} (days)	t_{meas} (days)
Sample without Cd	809.0	8.11
Sample with Cd	825.8	8.17

Figures 3–5 show the specific gamma lines and the Gaussian fits for the 803-, 265.6-, and 304.6-keV lines, respectively, where the (a) panels show the gamma line for the sample without the cadmium shield, and the (b) panels show the gamma line for the sample with the cadmium shield. For both the 265.6 and the 304.6 line, a second gamma close to the gamma of interest was also included in the fit to correctly define the background under the Gaussian. The small 264.0-keV peak at the tail of the 265.6-keV gamma in Fig. 4 comes

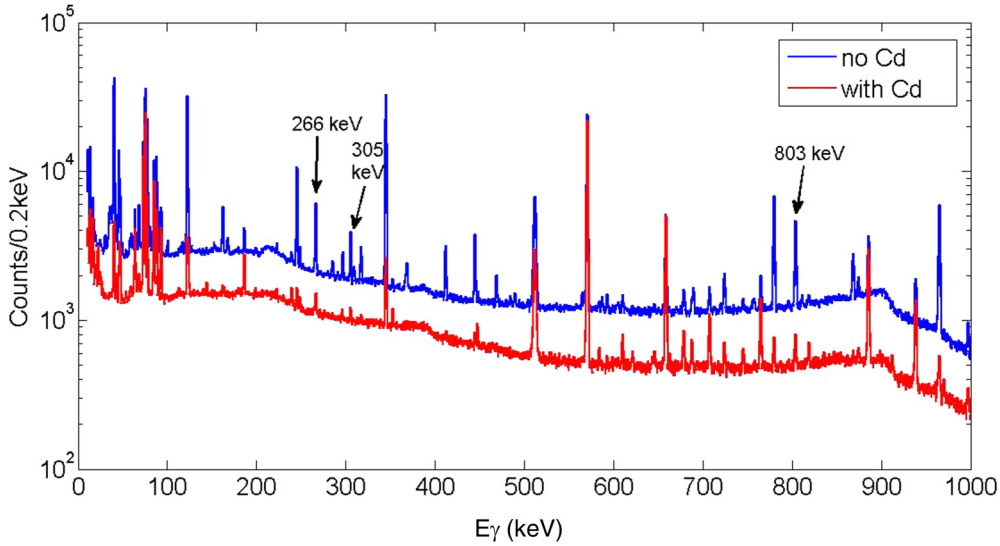

FIG. 2. Gamma spectra for irradiated bismuth samples without cadmium shield (blue, above) and with cadmium shield (red, below), acquired 2.23 yr after irradiation, showing the 803 line from ^{210g}Bi $\xrightarrow{\beta}$ ^{210}Po $\xrightarrow{\alpha}$ ^{206*}Pb decay, and 265.6 keV and 304.6 keV lines from ^{210m}Bi $\xrightarrow{\alpha}$ ^{206*}Tl decay.

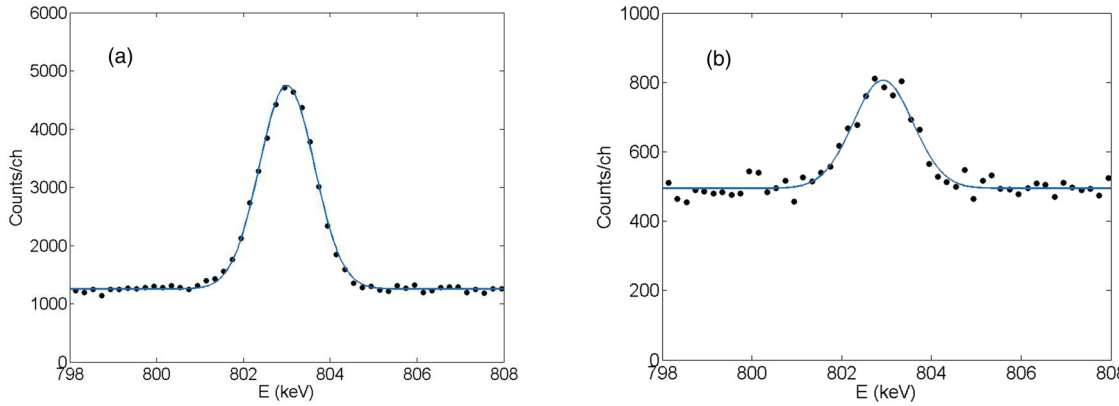

FIG. 3. Measured 803 keV gamma line with fit, (a) bismuth sample with no cadmium shield, (b) bismuth sample with cadmium shield.

from neutron capture on impurities of tantalum, leading to activation of ^{182}Ta with a 114-day half-life, emitting several gammas, all of which are observed in the activation spectrum. Likewise, near the 304.6-keV peak in Fig. 5 is seen a 308.5-keV contamination from decay of ^{192}Ir with a 73.8-day half-life. In both cases, the 2.23-yr cooling period provided for sufficient decay to allow accurate measurement of the 265.6- and 304.6-keV lines. It should be emphasized the activity of the 265.6- and 304.6-keV lines remained constant over the several measurements spanning 4 yr. Table III lists the total counts in each gamma line obtained from the fits in Figs. 3–5, for both the bismuth samples with and without the cadmium shield.

IV. HPGe DETECTOR EFFICIENCY: MEASUREMENTS AND SIMULATIONS

The gamma activity of the irradiated bismuth samples was measured with a HPGe purchased from Ortec-Ametek [20], with nominal efficiency of 31% with respect to a 2-in. × 2-in. NaI. The detector was of the GMX series noted for neutron damage resistance due to the coaxial geometry and *n*-type active region, and good efficiency even at low gamma energies down to 5-keV gammas due to the 0.5-mm beryllium window and outer contact consisting of a 0.3-μm boron implant. Radiographic studies were performed with a microfocus x-ray system to accurately measure the active volume and the exact placement of the germanium crystal in the HPGe detector enclosure, found to be consistent with the specifications provided by the detector manufacturer. The horizontal cryostat configuration of the detector required construction of a special holder that enabled placing the activated bismuth samples on axis and on contact with the detector enclosure in a reproducible fashion to obtain maximum accuracy and detection efficiency for the gammas. The detector window was concave due to the difference in pressure (vacuum inside) and therefore a holder was necessary to mount the irradiated sample in contact with the detector surface in a reproducible fashion.

The HPGe detector efficiencies were determined with detailed Geant4 [21] simulations of the detector with the known geometry and physical processes, including gamma interaction and reinteraction in the detector volume, and the target self-absorption due to the bismuth disk and sample holder. To corroborate the efficiency calculations and verify correct knowledge of the detector geometry, efficiency measurements were performed with the 662-keV line of a calibrated ^{137}Cs source, and the 1173- and 1332-keV lines of a ^{60}Co calibration source. The calibration sources were point sources and were placed on axis at a distance of 5 cm from the surface of the detector encapsulation. Detector efficiency for each gamma energy was determined taking into account the certification date, calibrated activity, gamma line branching ratio, and

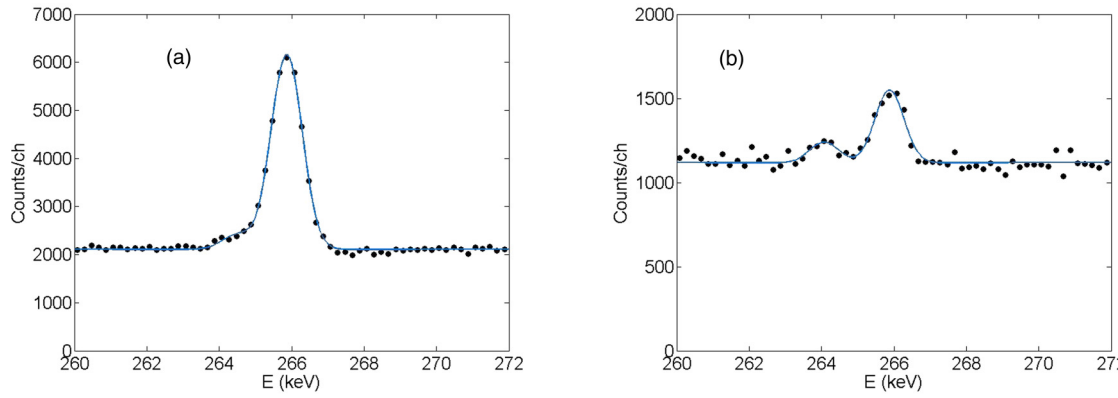

FIG. 4. Measured 265.6 keV gamma line with fit, (a) bismuth sample with no cadmium shield, (b) bismuth sample with cadmium shield.

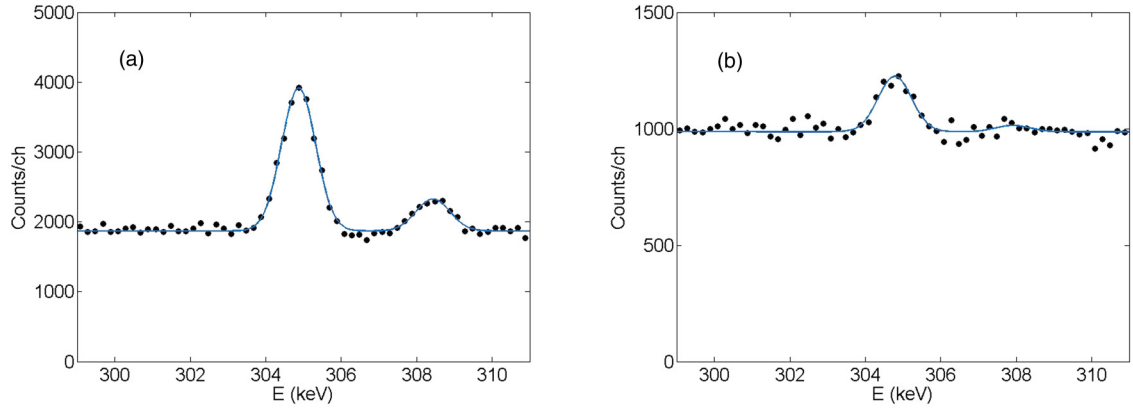

FIG. 5. Measured 304.6 keV gamma line with fit, (a) bismuth sample with no cadmium shield, (b) bismuth sample with cadmium shield.

radionuclide half-life. The measured detector efficiencies were then compared to the calculated efficiencies, where for the ^{60}Co source the simulation included the possibility of both simultaneous gamma lines interacting in the detector, thereby effectively lowering the detector efficiency for the calibrated source. Table IV lists the comparison between the simulations and the actual measurements.

Table V lists the calculated detector efficiencies for the bismuth samples in the special holder placed in contact with the detector window. The simulations include exact detector geometry and holder distance as described above. Self-absorption of the gammas in the bismuth sample as well as absorption in the beryllium window are included. The estimated errors are ±5% due to the uncertainty in the exact placement of the sample holder. It should be emphasized that the ratio between efficiencies for the 803-keV gamma and for the 256.6- and 304.6-keV gamma—used for extracting the σ_g/σ_m ratios—has a very weak dependence on HPGe detector geometry and/or source distance.

V. ANALYSIS AND RESULTS

A. Derivation of the activation cross-section ratios σ_g/σ_m, with thermal and epithermal neutrons

For each of the bismuth samples, the total number of activated ^{210g}Bi atoms from the irradiation was determined from the counts in the 803-keV gamma peak, as given by the following formula (derivation appears in the Appendix):

$$S^{\rm meas}_{\rm Bi210g} = N_{\rm Bi210g} \times \left(\frac{t_{\rm meas}}{\tau_\alpha}\right) \times \frac{\lambda_\beta}{\lambda_\beta - \lambda_\alpha} \times \varepsilon_\gamma \times I_\gamma \times f^{\alpha}_{\rm meas} \times \sum_{i=1}^{3} f_i\left[f^{i,\alpha}_{\rm irr} \exp\left(-\lambda_\alpha t_i\right) - f^{i,\beta}_{\rm irr} \exp\left(-\lambda_\beta t_i\right)\right]. \quad (1)$$

TABLE III. Measured counts for gammas from ^{210g}Bi and ^{210m}Bi ≈2.2 yr after irradiation.

	803 keV	265.6 keV	304.6 keV
$S_{\rm no\ Cd}$	27 610 ± 270	21 665 ± 215	11 550 ± 216
$S_{\rm with\ Cd}$	2 611 ± 126	2 166 ± 135	1 317 ± 113

$S^{\rm meas}_{\rm Bi210g}$ is the total measured counts obtained from the fit of the 803-keV peak with the bismuth sample. $N_{\rm Bi210g}$ is the total number of ^{210g}Bi atoms produced during reactor irradiation, $\lambda_\beta = 1/\tau_\beta$ is the decay constant of ^{210g}Bi → ^{210}Po + β^-, and $\lambda_\alpha = 1/\tau_\alpha$ is the decay constant of ^{210}Po → ^{206}Pb + α. $\varepsilon_\gamma = 0.0395 \pm 0.0020$ is the γ efficiency for the 803-keV line with the sample in contact with the HPGe detector, including sample and holder geometry and bismuth sample self-absorption as determined by detailed Geant4 simulations. I_γ is the probability for ^{210}Po emitting the 803-keV gamma, and includes the branching ratio for the 803-keV gamma line while taking into consideration the probability of electron conversion, or $I_\gamma = I_{\rm b.r.} \times I_{\rm ec}$. We take as the branching ratio the value obtained from our previous measurement [15], $I_{\rm b.r.} = (1.15 \pm 0.09) \times 10^{-5}$. The correction for electron conversion for the 803-keV line is $I_{\rm ec} = (0.9920 \pm 0.0002)$. The time $t_{\rm i}$ is taken from the end of the irradiation number i to the beginning of the gamma measurement period. The fraction for the ith irradiation, compared to the total irradiation, is given by f_i, and the correction factor $f^i_{\rm irr}$ is the correction for ^{210g}Bi beta decay or ^{210}Po alpha decay during irradiation number i, for example $f^{i,\alpha}_{\rm irr} = [1 - \exp(-\lambda_\alpha t^i_{\rm irr})]/\lambda_\alpha t^i_{\rm irr}$. Decay during the measurement is given by $f^{\alpha}_{\rm meas} = [1 - \exp(-\lambda_\alpha t_{\rm meas})]/\lambda_\alpha t_{\rm meas}$.

For a time much longer than the beta decay time, or $\tau_i \gg 1/\lambda_\beta$, the second term in brackets in Eq. (1) can be neglected. Also, for short irradiation times, α decay during irradiation can be neglected. Equation (1) can be simplified, where $t_{\rm cool}$ is the cooling time from the end of the last irradiation to beginning of gamma measurement;

$$S^{\rm meas}_{\rm Bi210g} = N_{\rm Bi210g} \times \frac{\lambda_\beta}{\lambda_\beta - \lambda_\alpha} \times \varepsilon_g \times I_g \times D_{\rm irr} \times \left[1 - \exp\left(-\lambda_\alpha t_{\rm meas}\right)\right] \times \exp\left(-\lambda_\alpha t_{\rm cool}\right), \quad (2)$$

TABLE IV. Measured and calculated HPGe efficiencies for the calibration sources

Gamma Energy (keV)	Measured Efficiency: Point source @ 5 cm	Calculated Efficiency: Point Source @ 5 cm
662	0.0082 ± 0.0003	0.00792
1173	0.00491 ± 0.00015	0.00487
1332	0.00443 ± 0.00013	0.00437

TABLE V. Calculated HPGe efficiencies for bismuth discs at contact with HPGe detector for the gammas from ^{210}Bi decay.

Gamma Energy (keV)	Calculated Efficiency: Bi disc on contact
265.6	0.0952 ± 0.0048
304.6	0.0881 ± 0.0044
803	0.0395 ± 0.0020

where $D_{\rm irr} = \sum_{i=1}^{3} f_i f_{\rm irr}^{i,\alpha} \exp(-\lambda_\alpha \Delta t_i)$, and $\Delta t_i = (t_i - t_{\rm cool})$.

For the number of bismuth atoms activated to the metastable state ^{210m}Bi, the calculation is much simpler given the long half-life of the metastable state of $\tau_{1/2} \approx 3$ million yr; the equation becomes ($t_m = \tau_{1/2}/\ln 2$)

$$S^{\rm meas}_{\rm Bi210m} = N_{\rm Bi210m} \times \frac{t_{\rm meas}}{\tau_m} \times \varepsilon_\gamma \times I_\gamma. \quad (3)$$

The probability for the ^{210m}Bi decay to emit the 265.6- and 304.6-keV gammas can be found in Ref. [22]. Table VI lists the parameters relevant for each of the gamma lines.

The recommended probabilities for the 265.6- and 304.6-keV gamma lines following ^{210m}Bi decay are found in the Nuclear Data Sheets (Kondev [22]). The values provided are 51% and 28% correspondingly, but errors are not provided. We have studied the original data in the literature (Tuggle [23]). We have also performed an independent evaluation of the branching ratios using the branching ratios and level feedings as reported in Ref. [23], and we obtain somewhat different branching ratios of 48.5% and 29% respectively. Our evaluation gave us an indication of the possible error involved in the gamma probabilities. We nevertheless used the recommended branching ratios provided by Kondev in the analysis below (Table VI). We estimate systematic errors of ≈7% for the gamma probabilities (statistical errors in Ref. [23] are very small). The uncertainties above are conservative, since the sum of the two transitions varies by only 1% and that by averaging over the yields of the two gammas we are essentially only sensitive to the uncertainty of this sum.

The measured counts for the 803 keV and quantities in Eq. (2) provide the total activation to ^{210g}Bi for the both bismuth samples at the end of irradiation,

$$(N_g)_{\rm no\ Cd} = (8.71 \pm 0.77) \times 10^{13} \text{ atoms}$$
$$(N_g)_{\rm with\ Cd} = (0.89 \pm 0.09) \times 10^{13} \text{ atoms}$$

From this we obtain the total activation to the ^{210g}Bi ground state from thermal and epithermal neutrons:

$$(N_g)_{\rm th} = [(N_g)_{\rm no\ Cd} - (N_g)_{\rm with\ Cd}]$$
$$= (7.82 \pm 0.69) \times 10^{13} \text{ atoms},$$
$$(N_g)_{\rm epi} = (N_g)_{\rm with\ Cd} = (0.89 \pm 0.09) \times 10^{13} \text{ atoms}.$$

The number of activated atoms as measured by the counts for the gammas from the ^{210m}Bi isomer state, due to the 265.6- and 304.6-keV gammas, are as follows:

$$\left(N_m^{266}\right)_{\rm no\ Cd} = (8.81 \pm 0.74) \times 10^{13} \text{ atoms},$$
$$\left(N_m^{305}\right)_{\rm no\ Cd} = (9.25 \pm 0.80) \times 10^{13} \text{ atoms},$$
$$\left(N_m^{266}\right)_{\rm with\ Cd} = (0.875 \pm 0.091) \times 10^{13} \text{ atoms},$$
$$\left(N_m^{305}\right)_{\rm with\ Cd} = (1.05 \pm 0.125) \times 10^{13} \text{ atoms}.$$

The total activation to ^{210m}Bi for the two bismuth samples at the end of irradiation, as derived from weighted average from the measured counts of the 265.6- and 304.6-keV peaks and parameters in Eq. (3), is

$$(N_m)_{\rm th} = (8.06 \pm 0.54) \times 10^{13} \text{ atoms},$$
$$(N_m)_{\rm epi} = (0.936 \pm 0.066) \times 10^{13} \text{ atoms}.$$

Combining these results, we get for the ratios of thermal to epithermal ^{210}Bi activation cross sections:

$$\left(\frac{\sigma_g}{\sigma_m}\right)_{\rm thermal} = \left(\frac{7.82 \pm 0.69}{8.06 \pm 0.54}\right) = 0.97 \pm 0.11,$$
$$\left(\frac{\sigma_g}{\sigma_m}\right)_{\rm epithermal} = \left(\frac{0.89 \pm 0.09}{0.934 \pm 0.074}\right) = 0.95 \pm 0.12.$$

B. Derivation of the bismuth thermal cross sections

Absolute thermal cross sections are obtained by comparison to a previous measurement of the thermal cross section reported by our group [15]. The measurement was obtained by simultaneous irradiation of bismuth samples and a gold foil in a reactor near-core location with a gold cadmium ratio of 9.0 accessed via a a pneumatic "rabbit" system. The irradiation for that measurement lasted 20 min. Two bismuth samples were simultaneously irradiated. A thin bismuth foil (on Mylar backing) was used for measuring the beta and alpha particles, the former from the ^{210g}Bi → ^{210}Po decay and the latter from the ^{210}Po → ^{206}Pb decay. A 1-mm-thick bismuth disk was used for measuring the 803-keV gamma line from the

TABLE VI. Parameters for extracting bismuth activation from gamma line intensities.

E_γ (keV)	Description	I_γ	ε_γ (contact)	$\tau_{1/2}$
803	^{210g}Bi → ^{210}Po→^{206}Pb+γ	$(1.14 \pm 0.09) \times 10^{-5}$	0.0395 ± 0.0020	5.012(5) days →138.3763(17) days
265.6	^{210m}Bi→^{206}Tl+γ	0.51 ± 0.036	0.0952 ± 0.0048	3.04 M yr
304.6	^{210m}Bi→^{206}Tl+γ	0.28 ± 0.020	0.0881 ± 0.0044	3.04 M yr

^{210}Po $\rightarrow$ ^{206*}Pb decay. The gold activation allowed a determination of the total neutron flux, which served as a normalization for determining the cross section for ^{210g}Bi activation with thermal neutrons. Details of the previous measurement can be found in Ref. [15]. A cross section of $(\sigma_g)_{\rm th} = 21.6 \pm 1.1$ mb was reported for activation to the ^{210g}Bi ground state by thermal neutrons.

For the present irradiation experiment near the reactor core, the two ampules were in close vicinity so that the two bismuth samples were irradiated with nominally identical neutron flux. The 0.5-mm cadmium shield covering the second ampule essentially absorbed the bulk of the thermal neutrons (at a 99% level), while allowing the epithermal neutrons to irradiate the enclosed bismuth sample. Making use of the presently measured ratio of $(\sigma_g/\sigma_m)_{\rm th}$ of 0.97 ± 0.11, we derive the following thermal cross sections for ^{210}Bi:

$$\begin{aligned}(\sigma_g)_{\rm th} &= 21.6 \pm 1.1 \text{ mb},\\ (\sigma_m)_{\rm th} &= 22.3 \pm 2.8 \text{ mb},\\ (\sigma_{\rm total})_{\rm th} &= 43.9 \pm 3.0 \text{ mb}.\end{aligned} \tag{4}$$

C. Bismuth average epithermal cross sections and resonant integral

An accurate measurement of the gold cadmium ratio can provide a measurement of the epithermal flux $\Phi_{\rm epi}$, in terms of the thermal flux $\Phi_{\rm th}$. The cadmium ratio is the ratio of activation of identical samples, one without and one with a cadmium shield. The cadmium ratio is given by

$$\mathrm{CR} = \frac{\bar{\sigma}_{\rm th} \times \Phi_{\rm th} + \bar{\sigma}_{\rm epi} \times \Phi_{\rm epi}}{\bar{\sigma}_{\rm epi} \times \Phi_{\rm epi}}, \tag{5}$$

where $\Phi_{\rm th}$ represents the thermal neutron flux (neutrons with $E_n < E_{\rm Cd}$), and $\Phi_{\rm epi}$ represents the epithermal neutron flux (neutrons with $E_n > E_{\rm Cd}$). We take the cadmium cutoff at $E_{\rm Cd} = 0.5$ eV. $\bar{\sigma}_{\rm th}$ is the average thermal cross section, where for a pure $1/v$ dependence of the cross section [24]

$$\bar{\sigma}_{\rm th} = \frac{\sqrt{\pi}}{2}\sigma_{\rm th} \tag{6}$$

with $\sigma_{\rm th} \equiv \sigma(2200\ \mathrm{m/s})$. Likewise, $\bar{\sigma}_{\rm epi}$ represents the average epithermal cross section, which in terms of the resonant integral is given by

$$\bar{\sigma}_{\rm epi} = \frac{\int_{0.5\ \mathrm{eV}}^{2\ \mathrm{MeV}} \sigma(E) \times \frac{1}{E} dE}{\int_{0.5\ \mathrm{eV}}^{2\mathrm{MeV}} \frac{1}{E} dE} = \frac{\mathrm{RI}}{\ln\left(\frac{2\,000\,000}{0.5}\right)} = \frac{\mathrm{RI}}{15.2}. \tag{7}$$

Equation (7) is applicable for an $1/E$ epithermal neutron energy distribution with a cutoff of 2 MeV, characteristic of water cooled reactors such as the Soreq IRR1 reactor.

From Eq. (5) we obtain

$$\Phi_{\rm epi} = \Phi_{\rm th} \times \frac{1}{(\mathrm{CR}_{\rm Au} - 1)} \times \left[\frac{(\bar{\sigma}_{\rm Au})_{\rm th}}{(\bar{\sigma}_{\rm Au})_{\rm epi}}\right]. \tag{8}$$

For gold, the thermal cross section and resonant integral have been accurately measured, with $(\sigma_{\rm Au})_{\rm th} = 98.7$ barns and $(\mathrm{RI})_{\rm Au} = 1571$ barns [25]. The average gold cross sections for the thermal and epithermal regions as derived from Eqs. (6) and (7) are therefore $(\bar{\sigma}_{\rm Au})_{\rm th} = 87.5$ barns and $(\bar{\sigma}_{\rm Au})_{\rm epi} = 103$ barns.

For the bismuth activation, the average cross sections are given by the number of activated ^{210}Bi atoms divided by the product of the density of ^{209}Bi atoms in the target times the neutron flux, or

$$(\bar{\sigma}_{\rm Bi210})_{\rm th} = \frac{(N_{\rm Bi210})_{\rm th}}{N_{\rm Bi209}\Phi_{\rm th}} \quad \text{and} \quad (\bar{\sigma}_{\rm Bi210})_{\rm epi} = \frac{(N_{\rm Bi210})_{\rm epi}}{N_{\rm Bi209}\Phi_{\rm epi.}}. \tag{9}$$

Putting together Eqs. (8) and (9), a good approximate for the average epithermal cross section in terms of the average thermal cross section is given by

$$(\bar{\sigma}_{\rm Bi210})_{\rm epi} \approx (\bar{\sigma}_{\rm Bi210})_{\rm th}\left[\frac{(N_{\rm Bi210})_{\rm epi}}{(N_{\rm Bi210})_{\rm th}}\right]\left[\frac{(\bar{\sigma}_{\rm Au})_{\rm epi}}{(\bar{\sigma}_{\rm Au})_{\rm th}}\right](\mathrm{CR}_{\rm Au} - 1). \tag{10}$$

Equations (8)–(10) are relevant for both the ^{210g}Bi and the ^{210m}Bi cases.

The gold cadmium ratio in the vicinity of irradiation of the two bismuth samples was measured shortly after removing the bismuth samples, yielding a ratio of 3.1. This confirmed the previously measured 3.1 gold cadmium ratio in this vicinity near the reactor core. Given the 7.5% uncertainty ($\approx 1\sigma$) of the reactor neutron flux due to possible fluctuations of the reactor power level, we assume possible error of 7.5% in the measured cadmium ratio. Corrections to Eqs. (5) and (10) are insignificant for gold and for bismuth for the accuracy desired here, the cadmium shield blocks off the thermal neutrons to a good approximation, and the Wescott g factor [25] is essentially 1 for both gold and bismuth since there is a $1/v$ characteristic in both cases and there are no resonances near the cadmium cutoff.

Equation (10) is applied to the activation measurements for the ground state and metastable states separately, to obtain the average cross sections in the epithermal neutron energy region:

$$\begin{aligned}(\bar{\sigma}_g)_{\rm epi} &= 5.4 \pm 0.9 \text{ mb},\\ (\bar{\sigma}_m)_{\rm epi} &= 5.7 \pm 1.0 \text{ mb}.\end{aligned}$$

The total average cross section in the resonance region is then given by

$$(\bar{\sigma}_{\rm total})_{\rm epi} = (\bar{\sigma}_g)_{\rm epi} + (\bar{\sigma}_m)_{\rm epi} = 11.1 \pm 1.3 \text{ mb}.$$

The resonant integral obtained for bismuth from the epithermal activation is then

$$RI_{\rm bismuth} = 169 \pm 20 \text{ mb}.$$

VI. DISCUSSION

The bismuth thermal capture cross sections presented in this work and based on our previous reported measurement [8] are compared to published measurements performed over the past several decades. Table VII (adopted from Borella *et al.* [1]) lists measurements employing techniques including the earlier pile oscillation experiments, γ and α activation and off-line measurements, detection of prompt gammas including

TABLE VII. Comparison of measurements and evaluations for thermal neutron capture cross section for bismuth (table adopted from reference [1]).

Measurement	Ref	Method	$(\sigma_g)_{th}$ mb	$(\sigma_g)_{epi}$ mb	$(\sigma_g)_{tot}$ mb
Shor *et al.* (2018)	[15]	Activation γ	21.6 (1.1)		
This work + Ref. [15].		**Activation γ**		**22.3 (2.8)**	**43.9 (3.0)**
Harris (1950)	[26]	Pile oscillator			38.0
Littler and Lockett (1953)	[27]	Pile oscillator			30.8(2.2)
Horsely (1956)	[28]	Pile oscillator			38–39
Tattersall *et al.* (1960)	[29]	Pile oscillator			36(4)
Seren *et al.* (1947)	[30]	Activation	15.0 (3.0)		
Colmer and Littler (1950)	[31]	Activation	20.5 (1.1)		
Takiue and Ishikawa (1978)	[32]	Activation	24.2 (0.4)		
Letourneau *et al.* (2006)	[33]	Activation α,γ	17.9 (0.8)		
Al-Khasawneh *et al.* (2021)	[2]	Activation α	16.2 (0.97)		
Stan-Sion *et al.* (2007)	[34]	AMS		21.3 (0.9)	
Tsai *et al.* (1984)	[35]	Primary γ's			$\geqslant$ 35.0
Sheline *et al.* (1989)	[36]	Primary γ's			$\geqslant$ 36.8
Letourneau *et al.* (2002)	[37]	Primary γ's			$\geqslant$35.0 (1.8)
Borella *et al.* (2011)	[1]	Primary γ's			$\geqslant$34.9 (0.7)
Sheline *et al.* (1989)	[36]	Total Energy			$\geqslant$36.8
Borella *et al.* (2011)	[1]	Total Energy			$\geqslant$37.6(0.9)
Borella *et al.* (2011)	[1]	Feeding γ	$\geqslant$21.4 (0.8)	$\geqslant$18.2 (0.7)	$\geqslant$39.6 (1.0)
Sheline *et al.* (1989)	[36]	Feeding γ	$\geqslant$19.7 (3.8)	$\geqslant$18.5 (3.2)	$\geqslant$38.2
Letourneau *et al.* (2002)	[37]	Feeding γ	$\geqslant$17.9 (2.0)	$\geqslant$17.1 (2.0)	$\geqslant$35
Domingo-Pardo *et al.* (2006)	[4]	Extrapolation from tails of resonances			23.6(0.9)

primary γ rays and feeding γ rays, total energy measurements, and accelerator mass spectrometry (AMS) study of the metastable state. Measurements of primary γ rays and feeding γ rays, along with total energy measurements, all report lower limits consistent with the measurements reported in this work. The activation measurements for $(\sigma_g)_{th}$, including the most recent Ref. [2], exhibit a significant disparity, despite the seemingly small error bars reported for each measurement. Our previous results for bismuth activation by thermal neutrons to the ^{210g}Bi ground state [15] lies between the reported activation measurements. The AMS measurement of the metastable state reported by Stan-Sion is consistent with that reported in this work for $(\sigma_m)_{th}$. The evaluated values for the total thermal capture cross sections, based on older pile oscillator data, are significantly lower than those reported here. The value reported by Domingo-Pardo *et al.* [4], based on extrapolation from tails of the measured bismuth resonances, provides a value for the total thermal cross section lower than all other results. As this method ignores the contributions of negative resonances, or equivalently of the direct capture process, this value should be taken as a lower limit.

A significant effort has been dedicated to determine the ratio (σ_g/σ_m) of neutron capture leading to the ^{210}Bi ground state relative to the ^{210}Bi metastable state. Neutron capture on ^{209}Bi forms a compound nucleus with an excitation energy of 4604 keV above the ^{210}Bi ground state (plus the E_n of the captured neutron). The metastable isomer is only 271 keV above the ground state, but the ^{210g}Bi has spin parity 1^- while the ^{210m}Bi isomer has spin-parity 9^-. It is therefore not clear that the prompt gamma cascade following neutron capture will populate the ground state and metastable isomer equally, despite the small energy difference.

The ratio $(\sigma_g/\sigma_m)_{th}$ for bismuth activation with thermal neutrons has been measured by several groups. Borella *et al.* [1] have performed measurements of prompt gamma rays with a bismuth target in thermal beam line in the Budapest Neutron Center reactor. They reported lower limits for the thermal capture leading to the ^{210g}Bi ground state and ^{210m}Bi metastable state, resulting in a ratio for $(\sigma_g/\sigma_m)_{th}$ of 1.18 with a 7% uncertainty. Letourneau *et al.* [37] have also reported lower limits for thermal neutron capture cross section, resulting in a ratio $(\sigma_g/\sigma_m)_{th}$ of 1.05 with a 15% uncertainty. Sheline *et al.* [36] have reported a ratio of 1.065 with a 30% uncertainty. In this work, we report a ratio $(\sigma_g/\sigma_m)_{th}$ of 0.97 $\pm$ 0.11 for thermal neutron capture on bismuth, consistent with equal population of the ^{210}Bi ground and metastable states, and consistent with the measurements performed previously for thermal neutrons. There is, however, a strong divergence in the prediction of evaluated libraries. The JENDL/A-96 (1992) library predicts overproduction of ^{210g}Bi, as well as the ROSFOND-2010

TABLE VIII. Comparison of measurements and evaluations for the branching ratio of $(\sigma_g/\sigma_m)_{th}$ for thermal neutron capture cross sections on bismuth

Measurements	Ref	$(\sigma_g/\sigma_m)_{th}$
This work		**0.97(11)**
Letourneau *et al.* 2002)	[37]	1.05(17)
Borella *et al.* (2011)	[1]	1.18(6)
Sheline *et al.* (1989)	[36]	1.065(31)
Evaluations		
JENDL/A-96 (1992)	[43]	≈ 8
ROSFOND-2010	[44]	≈ 2
JENDL-4.0	[45]	≈ 1
JEFF-3.2	[46]	≈ 1
BROND-3.1	[47]	≈ 1

evaluation library. The more recent evaluation libraries are in good agreement with the experimental results. A summary of the various measurements and evaluations for the ratio $(\sigma_g/\sigma_m)_{\rm th}$ is presented in Table VIII.

An effort has been made to determine the ratio of activation to ground state versus metastable state for neutron capture on bismuth for epithermal neutrons and for astrophysical relevant neutron energies. Saito *et al.* [40] measured bismuth capture for 30 keV neutrons, with off-line measurements to determine activation of the bismuth ground state, and prompt gamma TOF to determine population of the metastable state. They arrived at a (σ_g/σ_m) ratio of 3 ± 2. More recently, Shor *et al.* [8] have performed an activation measurement with a Maxwellian-like neutrons distribution from the $p +$ Li reaction to obtain the MACS for activation to the ^{210g}Bi of $(\sigma_g)_{\rm MACS} = 1.84 \pm 0.09$ mb. They compared their results to data in the literature for TOF measurements of the ^{210}Bi resonances, where the MACS for $(\sigma_g + \sigma_m)_{\rm MACS}$ was determined by convoluting the resonance data with a Maxwellian distribution. Taking the average of three MACS measurements by Domingo-Pardo *et al.* [4] with the nTOF facility, by Mutti *et al.* [41] at Gelina, and Beer *et al.* [42], Shor *et al.* [8] arrived at a $(\sigma_g/\sigma_m)_{\rm MACS}$ of 2.14 ± 1.07 for Maxwellian neutron at $kT = 30$ keV. The measurements presented in this current work report a ratio of $(\sigma_g/\sigma_m)_{\rm epi} = 0.95 \pm 0.12$ for bismuth activation by epithermal neutrons, consistent with the above ratios inferred for MACS measurements.

Figure 6, adopted from Ref. [3], shows a plot comparing the various measurements and evaluations for the ratio of (σ_g/σ_m) for activation to ^{210}Bi for a variety of incident neutron energies and distributions. The measurements at thermal neutron energies have been discussed above and are all consistent with our results. The measurements and evaluations at epithermal neutron energies and in the bismuth resonance regions exhibit significant disparities. A word of caution regarding comparing these measurements of (σ_g/σ_m) at the bismuth resonances energies. The data reported by Saito [40] are derived from TOF measurements for average cross section over finite energy intervals at 30 and 534 keV. The data reported by Borella *et al.* [3] have been measured at Gelina via TOF and the reported (σ_g/σ_m) ratios at the specific ^{210}Bi resonance. The data reported in Ref. [8] are for (σ_g/σ_m) obtained from the

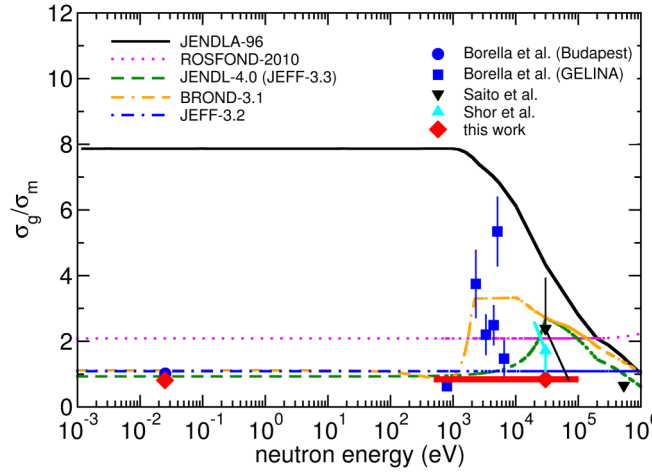

FIG. 6. Ratio of (σ_g/σ_m) for the reaction ^{209}Bi(n,γ)^{210}Bi as determined by: Evaluation studies [9,43–47], Activation measurements (this work and Borella *et al.* [1]), Ratios at individual resonances (Borella [3]) TOF measurements (Saito [40]) and MACS(Shor *et al.* [8]). Results of this work consistent with $(\sigma_g/\sigma_m) \approx 1$ at thermal and bismuth resonance energies.

MACS at 30 keV measured for activation to the ground state, compared to the average of several measurements for the total ^{210}Bi MACS cross section derived from bismuth resonance measurements. Also shown are the evaluated ratio (σ_g/σ_m), showing significant disparity among the various evaluated data, and a disparity with respect to the experimental data over whole energy range. A reassessment of the evaluated data may be warranted. The result of the present measurement for the $(\sigma_g/\sigma_m)_{\rm epi}$ ratio for epithermal neutrons is also shown in Fig. 6, highlighting the energy interval contributing most significantly to this measurement. The main conclusion of our measurements is that the average value of the ratio (σ_g/σ_m) for ^{210}Bi activation remains constant at about ≈1 for neutron energies at thermal energy, and over the energy range of the ^{210}Bi resonances.

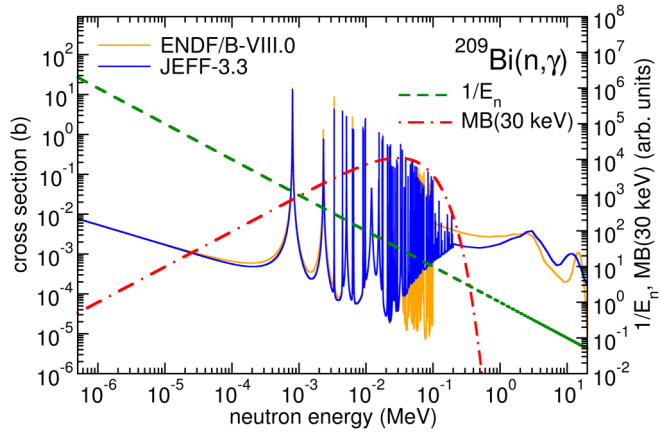

FIG. 7. Overlap of ^{210}Bi resonances with Maxwell-Boltzmann(MB) distribution at $kT = 30$ keV and reactor epi-thermal $1/E_n$ distribution (MB and $1/E_n$ at arbitrary scales).

TABLE IX. Bismuth Resonance integral $(RI)_{\text{bismuth}} = \int_{E_1}^{E_2} \sigma(E) \times \frac{1}{E} dE$ for several ranges of neutron energies. Bismuth resonances taken from JEFF-3.3 [39] evaluation.

Energy Range E_1 to E_2	$(RI)_{\text{bismuth}} = \int_{E_1}^{E_2} \sigma(E) \times \frac{1}{E} dE$ (mb)
(0.5 eV–2 MeV)	168
(0.5 eV–100 eV)	14
(0.5 eV–100 keV)	163
(0.5 keV–100 keV)	147
Thermal tail ($1/v$) above 0.5 eV	15
This work	**169(20)**

We argue that epithermal bismuth activation measurements in a reactor such as the Soreq IRR1 are relevant also for understanding astrophysical processes since the overlap with the bismuth resonances is in the same neutron energy interval as the Maxwellian distributions at $kT = 30$ keV, appropriate to the *s*-process reactions. Figure 7 shows ENDF [38] and JEFF [39] evaluated neutron resonant cross sections for bismuth, showing broad overlap with the Maxwell-Boltzmann neutron spectrum at a temperature of $kT = 30$ keV. Figure 7 also displays a $1/E_n$ distribution typical for epithermal neutrons in water cooled reactors. The $1/E_n$ convolution with the bismuth resonances shows a broad overlap with the Maxwell-Boltzmann distribution. Table IX demonstrates this observation in a more quantitative manner by listing the convolution of the bismuth resonances with the $1/E_n$ neutron distribution at various end points for the integral. The convolution of the bismuth resonances with the $1/E_n$ distribution is simply the resonance integral assuming different end points. Table IX demonstrates that the overwhelming contribution to the bismuth resonance integral is the in the neutron energy range 0.5–100 keV, the neutron energy region relevant for astrophysical *s*-process reactions. It is therefore our conclusion that the $(\sigma_g/\sigma_m)_{\text{epi}}$ ratio obtained for the bismuth epithermal activation in the reactor is also indicative of the $(\sigma_g/\sigma_m)_{\text{MACS}}$ ratio for bismuth activation with the Maxwellian neutrons at $kT \approx 30$ keV.

Finally, it is instructive to compare the cross-section results for Maxwell-Boltzmann (MB) and $1/E_n$ distributions obtained in this and our previous work [8,15] with other experimental data in the literature and with theoretical evaluation. For the $1/E_n$ distribution it is convenient also to present the resonance integral, which relates to the average cross section by scaling with the normalized factor of 15.2 [Eq. (7), appropriate for E_{max} 2 MeV]. The ^{209}Bi(n,γ) resonance cross sections for calculation of the resonance integral are taken from the ENDF/B-VIII.B4 and JEFF-3.3 libraries. These libraries are in good agreement with the experimental data also for the (σ_g/σ_m) ratio over most of the energy range (Fig. 6). Table X shows the numerical results for the convolutions of the bismuth resonances cross sections with the epithermal neutron energy distribution, and a comparison with experimental measurements. Table X also shows bismuth MACS calculated by convoluting the bismuth resonance cross sections with a Maxwellian distribution with $kT = 30$ keV, and a comparison with experimental data including our extrapolations for $(\sigma_m)_{\text{MACS}}$ assuming a $(\sigma_g/\sigma_m)_{\text{MACS}}$ ratio similar to that measured for epithermal bismuth resonant cross sections. As it is seen from the table, the results of our work are in a good agreement for both distributions, which supports the assumption for the $(\sigma_g/\sigma_m)_{\text{MACS}}$ branching ratio as in the epithermal region. It worthwhile to mention that the most recent measurement [2] is in good agreement with our results for both MB and $1/E_n$ distribution. On the other hand, the average values of three other measurements of $(\sigma_g)_{\text{MACS}}$ [2,6,7] yielding 2.01(38), 2.32(14), and 2.16(07), and three measurements of $(\sigma_{\text{tot}})_{\text{MACS}}$ [4,41,42] yielding 2.58(50), 2.54(48),

TABLE X. Bismuth activation with epi-thermal neutrons: Comparison of the evaluated and experimental cross-sections obtained for Maxwell-Boltzman and $1/E_n$ distributions. (* The MB cross-section for the isomer state σ_m for this work is evaluated under the assumption $(\sigma_g/\sigma_m)_{\text{epi}} = 0.95 \pm 0.12$ over the whole region of interest).

	Maxwell-Boltzman ($kT \approx 30$ keV)			Epi-thermal $\approx 1/E_n$		
	σ_{tot} (mb)	σ_g (mb)	σ_m (mb)	$\bar{\sigma}_{\text{Tot}}$ (mb) (RI_{Tot})	$\bar{\sigma}_g$ (mb) (RI_g)	$\bar{\sigma}_m$ (mb)(RI_m)
Shor *et al.* [8]		1.84 ± 0.09				
This work +Ref. [8]	*** 3.78 ± 0.28**		*** 1.94 ± 0.26**	**11.1 ± 1.3 (169)**	**5.4 ± 0.9 (82)**	**5.7 ± 1.0 (87)**
ENDF [38]	3.35			13.4 (204)		
JEFF [39]	2.95			11.0 (168)		
Domingo-Pardo [4]	2.58 ± 0.50					
Beer [42]	3.12 ± 0.6					
Mutti [41]	2.54 ± 0.48					
Ratzel [6]		2.32 ± 0.14				
Bisterzo [7]		2.16 ± 0.07				
Khasawne [2]		2.01 ± 0.38			5.9 (89.8)	

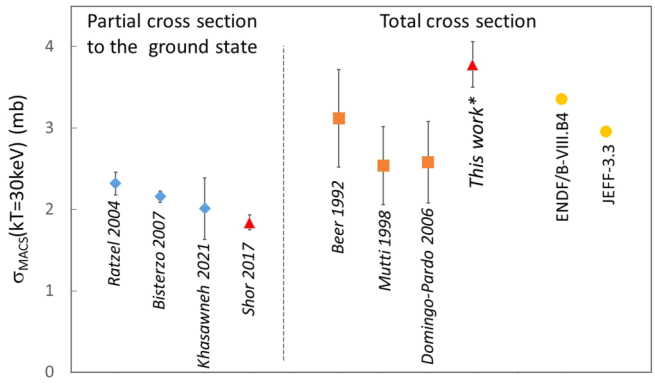

FIG. 8. Measurements of bismuth MACS at 30 keV for partial cross section to the ^{210}Bi ground state and total cross section. (* Total cross section for this work is based on previous measurement for the ground state [8], and current measurement of $(\sigma_g/\sigma_m)_{\rm epi} = 0.95 \pm 0.12$, and assuming same ratio for MACS.)

and 3.12(60), correspondingly, imply a (σ_g/σ_m) ratio 4.4(0.6). This is in strong contradiction with our conclusions and most of the evaluations (Fig. 6). A summary of the reported bismuth MACS at $kT = 30$ keV, for activation to the ^{210}Bi ground state, metastable state, and the total activation cross section is presented in Table X and displayed in Fig. 8. Our assessment for the total bismuth MACS cross section is $(\sigma_{\rm tot})_{\rm MACS} = 3.78 \pm 0.28$ mb. This is based on our previous measurement of partial cross section to the ^{210g}Bi ground state of $(\sigma_g)_{\rm MACS} = 1.84 \pm 0.09$ mb, and derived MACS for the metastable state of $(\sigma_g)_{\rm MACS} = 1.94 \pm 0.26$ mb, assuming $(\sigma_g/\sigma_m)_{\rm MACS} = (\sigma_g/\sigma_m)_{\rm epi} = 0.95 \pm 0.12$.

VII. SUMMARY

Activation measurements for the reaction ^{209}Bi$(n,\gamma)^{210}$Bi with both thermal and epithermal neutron distributions are presented. A comparison is made between activation to the ^{210g}Bi ground state and to the ^{210m}Bi metastable state. The activations were performed by irradiating two nearly identical bismuth samples at the Soreq IRR1 research reactor, one without and one with a cadmium shield. Off-line measurements of the 803-keV line from the ^{210g}Bi $\xrightarrow{\beta}$ ^{210}Po $\xrightarrow{\alpha}$ ^{206*}Pb reaction and the 265.6-keV line and the 304.6-keV lines from the ^{210m}Bi $\xrightarrow{\alpha}$ ^{206*}Tl reaction provide a measure of activation to the ^{210g}Bi ground state and the ^{210m}Bi isomer metastable state, respectively. Nearly equal levels of activation to the ground and to the metastable states of ^{210}Bi were observed, both for thermal and for epithermal neutron induced activations. For activation with thermal neutrons, a ratio of $(\sigma_g/\sigma_m)_{\rm th}$ of 0.97 ± 0.11 was obtained. The measurements with epithermal neutrons yield a ratio $(\sigma_g/\sigma_m)_{\rm epi}$ of 0.95 ± 0.12.

Absolute thermal cross sections for bismuth activation to ^{210}Bi were obtained by comparison to our previously reported measurements of $(\sigma_g)_{\rm th} = 21.6 \pm 1.1$ mb, resulting in a thermal activation cross section to the isomer state of $(\sigma_m)_{\rm th} = 22.3 \pm 2.8$ mb, together summing to a total activation cross section $(\sigma_{\rm tot})_{\rm th} = 43.9 \pm 3.0$ mb. The gold cadmium ratio measured at the irradiation site enabled derivation of the mean epithermal cross section for ^{210}Bi activation of $(\bar{\sigma}_g)_{\rm epi} = 5.4 \pm 0.9$ mb and $(\bar{\sigma}_m)_{\rm epi} = 5.7 \pm 1.1$ mb, and an inferred total resonant integral of $I_{\rm res} = 169 \pm 20$ mb. Knowledge of the level of activation of ^{210m}Bi is vital for GenIV reactor design due to the long lifetime of the isomer.

It is argued that the bismuth resonances lie in the neutron energy range relevant for stellar temperatures, and therefore measurements of epithermal activation are applicable also to astrophysical processes, most notably the ratio for σ_g/σ_m at stellar temperatures. With this assumption we conclude total bismuth MACS of $(\sigma_{\rm tot})_{\rm MACS} = 3.78 \pm 0.28$ mb, based on our previous measurement of $(\sigma_g)_{\rm MACS} = 1.84 \pm 0.09$ mb, and derived MACS for the metastable state of $(\sigma_g)_{\rm MACS} = 1.94 \pm 0.26$ mb, assuming $(\sigma_g/\sigma_m)_{\rm MACS} = (\sigma_g/\sigma_m)_{\rm epi} = 0.95 \pm 0.12$.

This work together with our previous measurements are compared to other experimental results in the literature and with evaluations from nuclear data libraries. The overall agreement is only partial, which calls for further improvements in the experimental and theoretical knowledge of neutron capture on bismuth and ^{210}Bi activation.

ACKNOWLEDGMENTS

We thank Prof. M. Paul for valuable comments and suggestions regarding this work and manuscript. We are also grateful to N. Hazenshprung, T. Makmal, and the Soreq reactor staff for their very dedicated operation of the Soreq reactor while accommodating this measurement. This research was made possible by joint EC-JRC and IAEC-Soreq collaboration and support.

APPENDIX

We derive formulas for irradiation of ^{209}Bi with a broad neutrons spectrum. For the sake of the analysis here $\sigma_g\Phi$ is used as shorthand for $\int_{E_1}^{E_2} \sigma_g \Phi' dE$, where the integral is over the energy range of choice. σ_g is the spectrum averaged cross section for producing ^{210g}Bi in the given flux spectrum Φ' in the incident neutron energy range $[E_1,\ E_2]$. Φ is then the total flux integrated over the energy range.

Three irradiations took place. In each irradiation, lasting for a time $t_{r,i}$, $N\sigma\Phi_i t_{r,i}$ ^{210g}Bi nuclei are produced, with N the number of ^{209}Bi nuclei in the sample. i is the irradiation number ($i = 1, 2, 3$). The total number of nuclides ^{210g}Bi that are produced is $N_g = N\sigma \sum_{k=1}^{3} \Phi_i t_{r,i}$. (In principle we should also account for variations in Φ_i from one irradiation to the next. Variations during reactor operation are very small and are neglected.) The fraction of nuclides produced in radiation i is $f_i = \frac{\Phi_i t_{r,i}}{\sum_{k=1}^{3} \Phi_i t_{r,i}}$. The time from the end of each irradiation to the start of the gamma measurement is t_i. The duration of the gamma measurement is t_m. The decay constant of ^{210g}Bi is $\lambda_1 = \ln(2)/5.012(5)d$. The decay constant of its daughter ^{210}Po is $\lambda_1 = \ln(2)/138.3763(17)d$. The emission probability for the 803-keV gamma-ray emitted by ^{210}Po is I_γ. Its detection efficiency is ϵ_γ.

During one of the irradiations the number n_1 of ^{210g}Bi builds up according to $\dot{n}_1 = -\lambda_1 n_1 + N\sigma_g\Phi$:

$$n_1(t) = \frac{N\sigma_g\Phi}{\lambda_1}(1 - e^{-\lambda_1 t}). \tag{A1}$$

The number n_2 of ^{210}Po builds up according to $\dot{n}_2 = -\lambda_2 n_2 + \lambda_1 n_1$:

$$n_2(t) = \frac{N\sigma_g\Phi}{\lambda_2}\left[\frac{\lambda_1}{\lambda_1 - \lambda_2}(1 - e^{-\lambda_2 t}) - \frac{\lambda_2}{\lambda_1 - \lambda_2}(1 - e^{-\lambda_1 t})\right]. \tag{A2}$$

This is verified by substituting into the differential equation and the check that $n_2(0) = 0$. For long irradiations the saturation value of $N\sigma_g\Phi/\lambda_2$ is attained, as also seen from setting $\dot{n}_1 = 0$ and $\dot{n}_2 = 0$ in the differential equations. Since the intensity of the irradiations is insufficient to alter the number of target nuclei to a significant degree, we can simply add the contributions of subsequent irradiations.

The number of measured counts $S = S_1 + S_2$ is then composed of two parts. The first part S_1 is due to the nuclides of ^{210}Po that were already formed during each irradiation. The second part S_2 is due to the nuclides of ^{210g}Bi that must first decay to ^{210}Po.

$$S_1 = \epsilon_g I_g(1 - e^{-\lambda_2 t_m})\sum_{i=1}^{3}\frac{N\sigma_g\Phi_i}{\lambda_2}e^{-\lambda_2 t_i} \times \left[\frac{\lambda_1}{\lambda_1 - \lambda_2}(1 - e^{-\lambda_2 t_{r,i}}) - \frac{\lambda_2}{\lambda_1 - \lambda_2}(1 - e^{-\lambda_1 t_{r,i}})\right]. \tag{A3}$$

If a is the number of nuclides of ^{210g}Bi at the end of an irradiation, then following an irradiation

$$n_1(t) = ae^{-\lambda_1 t} \quad \text{and} \quad n_2(t) = a\frac{\lambda_1}{\lambda_1 - \lambda_2}(e^{-\lambda_2 t} - e^{-\lambda_1 t}).$$

Then

$$S_2 = \epsilon_g I_g(1 - e^{\lambda_2 t_m})\sum_{i=1}^{3}\frac{N\sigma_g\Phi_i}{\lambda_1 - \lambda_2}(1 - e^{-\lambda_1 t_{r,i}})(e^{-\lambda_2 t_i} - e^{-\lambda_1 t_i}). \tag{A4}$$

Summing the two contributions gives

$$S = \epsilon_g I_g(1 - e^{-\lambda_2 t_m})\sum_{i=1}^{3}\frac{N\sigma_g\Phi_i}{\lambda_2}\left[\frac{\lambda_1}{\lambda_1 - \lambda_2}e^{-\lambda_2 t_i}(1 - e^{-\lambda_2 t_{r,i}}) - \frac{\lambda_2}{\lambda_1 - \lambda_2}e^{-\lambda_1 t_i}(1 - e^{-\lambda_1 t_{r,i}})\right]. \tag{A5}$$

Given the long cooling time in the present work (about 810 days) and the short half-life of ^{210g}Bi (5 days), the second term in square brackets can be neglected. To a very good approximation then

$$S \approx \epsilon_g I_g(1 - e^{-\lambda_2 t_m})\sum_{i=1}^{3}\frac{N\sigma_g\Phi_i}{\lambda_2}\frac{\lambda_1}{\lambda_1 - \lambda_2}e^{-\lambda_2 t_i}(1 - e^{-\lambda_2 t_{r,i}}). \tag{A6}$$

Introducing N_g and f_i as defined above, this becomes

$$S \approx \epsilon_g I_g N_g(1 - e^{-\lambda_2 t_m})\frac{\lambda_1}{\lambda_1 - \lambda_2}\sum_{i=1}^{3} f_i e^{-\lambda_2 t_i}\frac{1 - e^{-\lambda_2 t_{r,i}}}{\lambda_2 t_{r,i}}. \tag{A7}$$

For the present irradiation times the factor $(1 - e^{-\lambda_2 t_{r,i}})/\lambda_2 t_{r,i}$ equals 1–8 parts in 10^4, an approximation that is compatible with the present aim for uncertainty at the percent level. On the other hand, $(1 - e^{-\lambda_2 t_m})$ differs from $\lambda_2 t_m$ by -2%, so the approximation should not be made.

The above argument deducing S from S_1 and S_2 without further explanation could have been made more explicit by considering the decay after irradiation explicitly. Resetting time to 0 after irradiation ($r = N\sigma_g\Phi = 0$) and allowing then for both $n_1(0)$ and $n_2(0)$ to differ from 0, we get

$$n_1(t) = n_1(0)e^{-\lambda_1 t},$$
$$n_2(t) = n_2(0)e^{-\lambda_2 t} + n_1(0)\frac{\lambda_1}{\lambda_1 - \lambda_2}(e^{-\lambda_2 t} - e^{-\lambda_1 t}). \tag{A8}$$

This is again verified by substitution in the differential equations with $r = 0$ and by checking the initial values. Substituting for $n_1(0)$ and $n_2(0)$ the values at the end of the irradiation gives for $n_2(t)$

$$n_2(t) = e^{-\lambda_2 t}\left[\frac{r}{\lambda_2}(1 - e^{-\lambda_2 t_r}) - \frac{r}{\lambda_1 - \lambda_2}(e^{-\lambda_2 t} - e^{-\lambda_1 t}) + \frac{r}{\lambda_1 - \lambda_2}(e^{-\lambda_2 t} - e^{-\lambda_1 t})(1 - e^{-\lambda_1 t_r})\right],$$
$$n_2(t) = \frac{r}{\lambda_2(\lambda_1 - \lambda_2)}[e^{-\lambda_2 t}\lambda_1(1 - e^{-\lambda_2 t_r}) - e^{-\lambda_1 t}\lambda_2(1 - e^{-\lambda_1 t_r})]. \tag{A9}$$

The latter is simplified further by the fact that $\lambda_1 t \gg 1$ so that the second term may be neglected. In addition, the irradiation time is short compared to the half-life of the second decaying nuclide so that $(1 - e^{-\lambda_2 t_r}) \approx \lambda_2 t_r$ to 8 parts in 10^4. This gives

$$n_2(t) = rt_r\frac{\lambda_1}{(\lambda_1 - \lambda_2)}e^{-\lambda_2 t}, \tag{A10}$$

to better than 0.1% for the cooling and irradiation times considered here. Considering again three irradiations $N_g = \sum_{k=1}^{3} \mathrm{r}_i t_{r,i}$ and $f_i = \mathrm{r}_i t_{r,i}/\sum_{k=1}^{3} \mathrm{r}_i t_{r,i}$ we get

$$S \approx \epsilon_g I_g N_g(1 - e^{-\lambda_2 t_m})\frac{\lambda_1}{\lambda_1 - \lambda_2}\sum_{i=1}^{3} f_i e^{-\lambda_2 t_i}. \tag{A11}$$

[1] A. Borella, T. Belgya, S. Kopecky, F. Gunsing, M. Moxon, M. Rejmund, P. Schillebeeckx, and L. Szentmiklósi, Nucl. Phys. A **850**, 1 (2011).
[2] K. Al-Khasawneh *et al.*, Phys. Rev. C **103**, 065805 (2021).
[3] A. Borella *et al.*, *Int. Conf. on Nucl. Data for Science and Technology*, Nice, France, edited by O. Bersillon and F. Gunsing (EDP Sciences, 2007), pp. 563–566.
[4] C. Domingo-Pardo *et al.*, (nTOF Collaboration), Phys. Rev. C **74**, 025807 (2006).
[5] F. Käppeler, R. Gallino, S. Bisterzo, and W. Aoki, Rev. Mod. Phys. **83**, 157 (2011).
[6] U. Ratzel *et al.*, Phys. Rev. C **70**, 065803 (2004).
[7] S. Bisterzo, F. Käppeler, R. Gallino, M. Heil, C. Domingo-Pardo, C. Vockenhuber, and A. Wallner, Int. Conf. Nucl. Data Sci. Technol. ND2007 (EDP Sciences, CEA, 2008), pp. 1333–1336.
[8] A. Shor *et al.*, Phys. Rev. C **96**, 055805 (2017).
[9] A. J. M. Plompen *et al.*, Eur. Phys. J. A **56**, 181 (2020).
[10] The Lund/LBNL Nuclear Data Search Version 2.0, LBNL,Berkeley, 1999, nucleardata.nuclear.lu.se/toi/
[11] LNHB/CEA Table de Radionucleides (2014), http://www.nucleide.org/DDEP.htm, http://www.nucleide.org/Laraweb/
[12] H. Schatz, R. Toenjes, B. Pfeiffer, T. C. Beers, J. J. Cowan, V. Hill, and K.-L. Kratz, Astrophys. J. **579**, 626 (2002).
[13] D. Vandeplassche and L. Medeiros Romão, *IPAC2012, Applications of Accelerators* (IPAC12/IEEE, New Orleans, Louisiana, 2012), p. 6.
[14] A. C. Mueller, J. Phys.: Conf. Ser. **420**, 012059 (2013).
[15] A. Shor *et al.*, Phys. Rev. C **97**, 034303 (2018).
[16] A. Trkov and V. Radulovic, Radioanal. Nucl. Chem. **304**, 763 (2015).
[17] P. N. Son and V. H. Tan, SpringerPlus **5**, 863 (2016).
[18] IRR-1 reactor, Israel. https://www.osti.gov/servlets/purl/4459149
[19] https://www.princetonscientific.com/high_purity_materials
[20] https://www.ortec-online.com/products/radiation-detectors/germanium-hpge-radiation-detectors
[21] http://www.geant.org/Projects/GEANT_Project_GN4
[22] G. Kondev, Nucl. Data Sheets **109**, 1527 (2008).
[23] D. G. Tuggle, Ph.D. thesis, University of California at Berkeley, 1976, LBL-4460, https://escholarship.org/uc/item/2sq0k0md
[24] G. Feinberg *et al.*, Phys. Rev. C **85**, 055810 (2012).
[25] B. Pritychenko and S. F. Mughabghab, Nucl. Data Sheets **113**, 3120 (2012).
[26] S. P. Harris, C. O. Muehlhause, S. Rasmussen, H. P. Schroeder, and G. E. Thomas, Phys. Rev. **80**, 342 (1950).
[27] D. J. Littler and E. E. Lockett, Proc. Phys. Soc. A **66**, 700 (1953).
[28] G. W. Horsley, J. Nucl. Energy **6**, 41 (1957).
[29] R. B. Tattersall, H. Rose, S. K. Pattenden, and D. Jowitt, J. Nucl. Energy **A12**, 32 (1960).
[30] L. Seren, H. N. Friedlander, and S. H. Turkel, Phys. Rev. **72**, 888 (1947).
[31] F. C. W. Colmer and D. J. Littler, Proc. Phys. Soc. A **63**, 1175 (1950).
[32] M. Takiue and H. Ishikawa, Nucl. Instrum. Methods **148**, 157 (1978).
[33] A. Letourneau, G. Fioni, F. Marie, D. Ridikas, and P. Mutti, Ann. Nucl. Energy **33**, 377 (2006).
[34] C. Stan-Sion, A. Letourneau, H. Reithmeier, V. Lazarev, M. Enachescu, and E. Nolte, Nucl. Instrum. Methods Phys. Res. B **259**, 739 (2007).
[35] J. S. Tsai, T. J. Kennett, and W. V. Prestwich, Phys. Rev. C **27**, 2397 (1983).
[36] R. K. Sheline, R. L. Ponting, A. K. Jain, J. Kvasil, B. bu Nianga, and L. Nkwambiaya, Czech. J. Phys. B **39**, 22 (1989).
[37] A. Letourneau *et al.*, *Proceedings of the 11th International Symposim on Capture Gamma-Ray Spectroscopy*, Prague, Czech Republic, edited by J. Kvasil, P. Cejnar, and M. Krticka (World Scientific publishers, 2002) p. 734.
[38] ENDF/B-VIII.B4, U.S. Evaluated Nuclear Data Library,2017.
[39] Jeff-3.3 evaluation library, https://www.oecd-nea.org/dbdata/jeff/jeff33/
[40] K. Saito, M. Igashira, T. Ohsaki, T. Obara, and H. Sekimoto, *Proceedings of the 2002 Symposium on Nuclear Data*, JAERI, Tokai, Japan, pp. 1133–1137.
[41] P. Mutti, F. Corvi, K. Athanassopulos, H. Beer, and P. Krupchitsky, in *Proceedings of the International Symposium on Nuclear Astrophysics: Nuclei in the cosmos V, Volos, Greece*, edited by N. Prantzos and S. Harissopulos (Editions Frontières, Paris, 1988), p. 204.
[42] H. Beer, F. Voss, and R. R. Winters, Astrophysical J. Suppl. **80**, 403 (1992).
[43] Y. Nakajima, JNDC WG on Activation Cross Section Data: JENDL Activation Cross Section File, Proceedings of the 1990 Symposium on Nuclear Data, JAERI-M 91-032, p. 43 (1991), edited by M. Igashira and T. Nakagawa, https://wwwndc.jaea.go.jp/ftpnd/jendl/jact10.html
[44] RUSFOND-2010, Russian File of Evaluated Neutron Data, released in 2010, https://www.oecd-nea.org/janisweb/tree/N/RUSFOND-2010
[45] K. Shibata *et al.*, JENDL-4.0: A New Library for Nuclear Science and Engineering, J. Nucl. Sci. Technol. **48**, 1 (2011).
[46] https://www.oecd-nea.org/dbdata/jeff/
[47] A. I. Blokhin, E. V. Gai, A. V. Ignatjuk, I. I. Koba, V. N. Manokhin, and V. N. Pronyaev, *New version of neutron evaluated data library BROND-3.1*, Yad.Reak.Kinst. No. 2 p. 62 (2016), https://vant.ippe.ru/en/brond-3-1.html

Correction: The first column of Table VII contained a typographical error and has been fixed.